PAPER

Check for updates

γ-Al₂O₃ nanorods with tuneable dimensions – a mechanistic understanding of their hydrothermal synthesis†

T. E. Bell,[a] J. M. González-Carballo,[b] R. P. Tooze[b] and L. Torrente-Murciano ⓘ *[a]

This paper reports for the first time the size control of well-defined and morphologically pure alumina (γ-Al₂O₃) nanorods, presenting an economic and reproducible route for the manufacture of these materials with tuneable sizes for useful applications, for example serving as adsorbents, catalysts and catalyst supports. A detailed understanding of the different steps taking place during the hydrothermal synthesis has been deduced herein. Understanding the effect of temperature on the relative rates of these steps is essential for achieving size and morphology selectivity, but has often been overlooked in the literature. This systematic study identifies six distinct steps taking place during the synthesis: (1) formation of Al(OH)₃, (2) dissolution of Al(OH)₃ into hexameric based fragments (3) thermolysis at temperatures ≥ 170 °C into soluble AlOOH (boehmite) building blocks (4) formation of lamellar AlOOH sheets (5) scrolling into nanorod crystallites and subsequent oriented attachment into high aspect nanorods and (6) growth by Ostwald ripening to low aspect nanorods. The obtained AlOOH nanorods are converted into γ-Al₂O₃ with conservation of morphology by calcination at 500 °C. Nanorod formation (step 5) can only be achieved at temperatures ≥ 180 °C (after 20 hours). At 180 °C, growth of the rods (step 6) takes place simultaneously with their slow formation (step 5) leading to two distinct nanorod products with different aspect ratios. At higher temperatures (200 °C), the rate of formation (step 5) is fast, quickly reaching completion, allowing for substantial growth of the nanorods and resulting in a monomodal size distribution. Thus, we have identified that γ-Al₂O₃ rods with high aspect ratio can be selectively synthesised at 180 °C for ≥20 hours, while low aspect ratios are produced at 200 °C for ≥10 hours. In all cases, the average size of the nanorods increases linearly with prolonged reaction time due to their continuous growth.

1. Introduction

Ceramic materials such as, alumina (Al₂O₃), are inexpensive materials commonly used as catalyst supports in numerous industrial processes.[1] The widespread use of Al₂O₃ in heterogeneous catalysis has arisen from its high chemical and thermal stability as well as its desirable textural properties such as surface area, porosity and surface acidity/basicity.[2] The gamma polymorph is most commonly used for catalyst supports due to its high specific surface area.[3] Despite the widespread use of bulk γ-Al₂O₃, in recent years, the focus has shifted towards nanostructured materials since altering the morphology at the nanoscale can potentially lead to materials with distinct physical and chemical properties. In addition, morphology control enables the selective exposure of different crystal surfaces, which may have distinct interactions with metal active sites and

reactants. These specific interactions can be exploited to offer additional stability to metal nanoparticles when implementing nanostructured γ-Al₂O₃ as a catalyst support.

Several routes have been reported for the synthesis of nanostructured materials including hydrothermal,[3–13] sol–gel,[14–17] anodisation,[18–20] atomic layer deposition[21] and wet etching.[22] Amongst these, hydrothermal methods are popular as they are cheap, reproducible, simple and can be easily scaled up. There are numerous published reports of hydrothermal syntheses of γ-Al₂O₃ using structure directing agents (SDAs) such as surfactants[7–9] and polymers,[1,23] which function as a template. However, these additives can affect the product crystallinity and SDAs can be hard to remove completely from the final materials. As such, hydrothermal procedures capable of maintaining high product quality without SDAs are more desirable and are the focus of the work herein. An alternative technique to direct product morphology is the use of anions such as sulphate, chloride and nitrate, which can adsorb preferentially to particular crystal surfaces to inhibit growth in certain directions.[24] Since anions can be easily removed by washing, they do not compromise the quality of the product.

[a]Department of Chemical Engineering and Biotechnology, University of Cambridge, Philippa Fawcett Drive, Cambridge CB3 0AS, UK. E-mail: lt416@cam.ac.uk

[b]Sasol Technology UK, Purdie Building, North Haugh, St Andrews, KY16 9ST, UK

† Electronic supplementary information (ESI) available. See DOI: 10.1039/c7ra02590d

Table 1 Review of the hydrothermal syntheses of 1D AlOOH and γ-Al_2O_3 in acidic conditions in absence of polymer/surfactant[a]

Precipitant agent or base	pH	Temperature (°C)	Time (hours)	Morphology	Size (nm)		SA_{BET} (m^2 g^{-1})	Ref.
					Length	Diameter		
NaOH	3.5	200	20	Nanorod (γ-AlOOH)	260	27	46	3
NaOH	4	200	24	Nanorod (γ-AlOOH)	200–300	10–30	85	4
	5	200	24	Nanorod (γ-AlOOH)	200–300	10–30	24	
$C_6H_5NH_2$	—	200	24	Nanorod (γ-AlOOH)	300–700	25–40	—	25
$NaNH_2$	—	200	4–6	Lamellar (γ-AlOOH)	20–40	20–25	—	5
	—	200	12	Nanotube (γ-AlOOH)	100	2–5	—	
	—	200	20	Nanorod (γ-AlOOH)	<180	15–20	—	
NH_4OH	5	200	48	Nanorod (γ-AlOOH)	100–400	20–30	—	26
NH_3	5	200	48	Nanorod (γ-AlOOH)	140–320	—	—	27
$(NH_4)_2CO_3$	—	100	24	Nanorod (γ-Al_2O_3)	90–140	35–45	165	28
	—	100	36	Nanorod (γ-Al_2O_3)	90–140	35–45	152	
$HCO-N(CH_3)_2$	2.5	150	24	Nanorod (γ-Al_2O_3)	<50	$\sim$5	457	29
$(C_2H_5)_4N(OH)$	—	170	72	Nanofibre (γ-Al_2O_3)	300–1000	8–15	210	30

[a] — indicates information not provided.

The hydrothermal conditions used in the literature to synthesise 1D AlOOH and γ-Al_2O_3 without SDAs are summarised in Table 1. It is clear from our previous work[3] that an acidic medium is required to hydrothermally produce 1D nanostructures and the literature suggests at least 12 hours at temperatures exceeding 100 °C are needed. It is important to note that Table 1 includes data for both AlOOH and γ-Al_2O_3 materials. While AlOOH can be easily converted to γ-Al_2O_3 by calcination, the crystal lattice contraction resulting from its dehydration has an effect on its size, which should be taken into consideration when comparing sizes.

Despite the work in the area, the ability to synthesise nanostructured alumina with simultaneous control over the morphology and size has not yet been reported. For example, syntheses at 200 °C for 24 hours can produce γ-AlOOH nanorods of either 200–300 nm or 300–700 nm length as reported by Yang[4] and Ma et al.[25] respectively. We believe that the key to developing control of the 1D nanostructure size lies within the understanding of the mechanism.

In our previous work,[3] we demonstrated morphological control of γ-Al_2O_3 materials by varying the NaOH : Al ratio, producing morphologically pure 2D nanoplates and 1D nanorods in basic and acidic conditions respectively.[3] Herein, we focus on the size control of γ-Al_2O_3 nanorods by developing an understanding of the synthetic mechanism using a combination of ^{27}Al NMR and electron microscopy techniques. This work has led to the identification of distinct steps leading up to nanorod formation and growth, where variations in synthesis temperature and time leads to controlled γ-Al_2O_3 sizes. Subsequently, the mechanistic understanding presented herein can be applied to tailor the γ-Al_2O_3 nanorod size by controlling synthesis temperature and time, which was not previously possible with hydrothermal methods.

2. Experimental

2.1 Synthesis of γ-alumina nanorods

The hydrothermal synthesis of γ-Al_2O_3 has been previously reported.[3] In a typical synthesis, 20 mL of 1 M NaOH solution is added to an aqueous solution containing 9.6 g of $Al(NO_3)_3$·$9H_2O$ in a PTFE lined stainless steel autoclave. The reactant quantities correspond to a NaOH : Al molar ratio of 0.77 : 1 which is known from our previous work[3] to yield morphologically pure γ-Al_2O_3 nanorods after hydrothermal synthesis at 200 °C for 20 hours. The initial pH of this mixture is 3.5. The precursors are treated hydrothermally in an air-circulating oven for 10 to 80 hours at 150 to 200 °C. After this time, the autoclave vessel is naturally cooled down to room temperature and the resulting white γ-AlOOH precipitate and solution are separated by centrifugation (4000 rpm, 3 minutes). The solid product is dried overnight in a vacuum oven at 80 °C, crushed into a fine powder and calcined at 500 °C for 3 hours (3 °C min^{-1} rate). The final γ-Al_2O_3 product is washed with distilled water and dried.
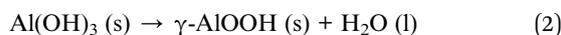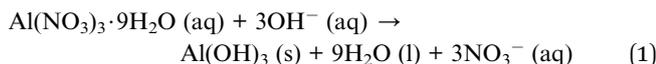
2.2 Characterisation

Transmission electron microscopy (TEM) was carried out using a JEOL JEM1200EXII instrument. Scanning electron microscopy (SEM) was carried out using a FEI Nova NanoSEM 450 using 5 kV accelerating voltage and 2.5 a.u. spot size at a working distance of 4.8 mm. Samples were sputter coated with approximately 6 nm layer of platinum to minimise charging. Exact platinum coating thickness was not determined and thus SEM is used for comparison and qualitative data of size and morphology rather than quantitative analysis. N_2 sorption measurements were carried out at −196 °C using a Micromeritics ASAP 2020 apparatus. All samples were degassed at 150 °C prior to analysis. Specific surface area was calculated using the BET method. Powder X-ray diffraction (pXRD) patterns were obtained using a Bruker D8 Advance diffractometer and a position sensitive VANTEC-1 detector with Cu Kα radiation, operated at 40 kV and 40 mA. ^{27}Al NMR experiments were run on a 500 MHz Bruker AV500 with 130.32 MHz resonance frequency, using a ca. 90 degree pulse, no proton decoupling (pulse sequence "zg"), spectral width of 500 ppm, acquisition time of 0.12 second, delay time of 1 second and 20 to 1200 scans for each experiment. All solutions were diluted in D_2O.
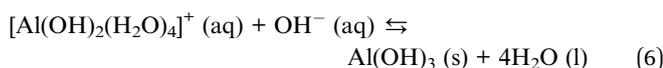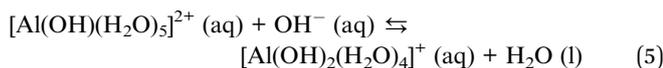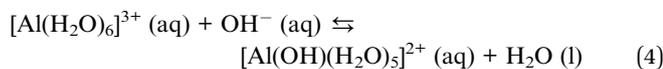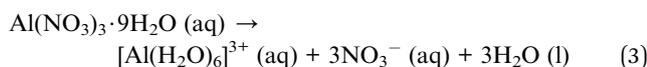
3. Results and discussion

3.1 Aluminium species involved in AlOOH formation

We have recently reported[3] that prior to hydrothermal synthesis of nanostructured alumina, addition of an aqueous solution of aluminium nitrate ($Al(NO_3)_3 \cdot 9H_2O$) to aqueous NaOH solutions leads to the formation of aluminium hydroxide solid ($Al(OH)_3$), according to reaction (1). We have also demonstrated that $Al(OH)_3$ is the precursor to the boehmite (γ-AlOOH) hydrothermal product (reaction (2)), which is converted into γ-Al_2O_3 by calcination at 400–700 °C.

$$Al(NO_3)_3 \cdot 9H_2O \ (aq) + 3OH^- \ (aq) \rightarrow$$
$$Al(OH)_3 \ (s) + 9H_2O \ (l) + 3NO_3^- \ (aq) \qquad (1)$$

$$Al(OH)_3 \ (s) \rightarrow \gamma\text{-AlOOH} \ (s) + H_2O \ (l) \qquad (2)$$

The morphology is conserved during this calcination step and consequently, the capacity to control the nanostructured γ-Al_2O_3 morphology and size is during the formation of γ-AlOOH step (reaction (2)).[3,6] Herein, we now develop upon this understanding, recognising intermediate steps taking place during these processes, providing useful insights on the overall mechanism of formation of γ-AlOOH nanorods, ultimately leading to nanorod size control.

The precise nature of the species resulting from hydrolysis of aluminium salts depends on a delicate balance of Al^{3+} concentration, base concentration, pH, degree of stirring, temperature, rate of base addition and aging time.[31] Further insights into the transformation of $Al(NO_3)_3 \cdot 9H_2O$ to $Al(OH)_3$ (reaction (1)), reveals that the conversion comprises of several intermediate steps. The process starts with the initial formation of $[Al(H_2O)_6]^{3+}$ cations (reaction (3)), easily susceptible to deprotonation as the small, highly charged Al^{3+} cation polarises and weakens the O–H bonds, resulting in sequential deprotonation to form aluminium monomers shown in reaction (4) and (5). It is worth noting that in an aqueous solution of aluminium nitrate, without the addition of base, the equilibrium position of reaction (4) and (5) is far to the left. However, the addition of base, such as NaOH, shifts the equilibria in reactions (4)–(6) towards the precipitation of solid $Al(OH)_3$.

$$Al(NO_3)_3 \cdot 9H_2O \ (aq) \rightarrow$$
$$[Al(H_2O)_6]^{3+} \ (aq) + 3NO_3^- \ (aq) + 3H_2O \ (l) \qquad (3)$$

$$[Al(H_2O)_6]^{3+} \ (aq) + OH^- \ (aq) \leftrightarrows$$
$$[Al(OH)(H_2O)_5]^{2+} \ (aq) + H_2O \ (l) \qquad (4)$$

$$[Al(OH)(H_2O)_5]^{2+} \ (aq) + OH^- \ (aq) \leftrightarrows$$
$$[Al(OH)_2(H_2O)_4]^+ \ (aq) + H_2O \ (l) \qquad (5)$$

$$[Al(OH)_2(H_2O)_4]^+ \ (aq) + OH^- \ (aq) \leftrightarrows$$
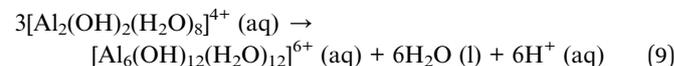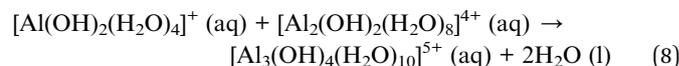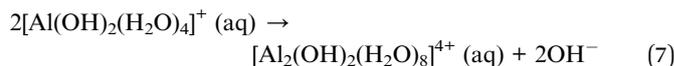$$Al(OH)_3 \ (s) + 4H_2O \ (l) \qquad (6)$$

The use of ^{27}Al NMR provides information about the species present in the reaction solution before and after hydrothermal treatment, facilitating unequivocal identification of any symmetrical aluminium species including monomers, dimers/

trimers and tridecamers.[32] Due to the quadrupolar nature of ^{27}Al, only symmetrical species are detected, resulting in a vast number of unidentifiable aluminium monomers, oligomers and polymers potentially present in solution.[33]

The formation of monomeric aluminium species by aqueous dissolution of $Al(NO_3)_3 \cdot 9H_2O$ is evidenced by ^{27}Al NMR spectra, shown in Fig. 1a. The peak at 0 ppm corresponds to all symmetrical, monomeric aluminium species in an octahedral arrangement including $[Al(H_2O)_6]^{3+}$, $[Al(OH)(H_2O)_5]^{2+}$ and $[Al(OH)_2(H_2O)_4]^+$.[31]

The mechanism of $Al(OH)_3$ formation by polymerisation of $[Al(OH)_2(H_2O)_4]^+$ cations (reaction (6)) is described in detail by reactions (7)–(9). In this process, the deprotonated monomers can dimerise, as shown for $[Al(OH)_2(H_2O)_4]^+$ in reaction (7) and subsequently, monomers and dimers can join to form trimers as in reaction (8). The dimers can aggregate into Al_6 hexamer rings ($[Al_6(OH)_{12}(H_2O)_{12}]^{6+}$) as shown in reaction (9). Further aggregation of the hexameric rings results in the precipitation of $Al(OH)_3$ which will be discussed in further detail later in this section but first the solution composition is examined.

$$2[Al(OH)_2(H_2O)_4]^+ \ (aq) \rightarrow$$
$$[Al_2(OH)_2(H_2O)_8]^{4+} \ (aq) + 2OH^- \qquad (7)$$

$$[Al(OH)_2(H_2O)_4]^+ \ (aq) + [Al_2(OH)_2(H_2O)_8]^{4+} \ (aq) \rightarrow$$
$$[Al_3(OH)_4(H_2O)_{10}]^{5+} \ (aq) + 2H_2O \ (l) \qquad (8)$$

$$3[Al_2(OH)_2(H_2O)_8]^{4+} \ (aq) \rightarrow$$
$$[Al_6(OH)_{12}(H_2O)_{12}]^{6+} \ (aq) + 6H_2O \ (l) + 6H^+ \ (aq) \qquad (9)$$

Upon the addition of NaOH to the aqueous solution of Al^{3+}, the formation of dimers/trimers (reactions (7) and (8)) and tridecamers ($[Al_{13}O_4(OH)_{24}(H_2O)_{12}]^{7+}$) in solution is evidenced by the ^{27}Al NMR peaks at 4.3 and 63 ppm respectively in Fig. 1b.[31,34] The formation of these species does not proceed in the absence of base under the studied conditions as shown by ^{27}Al NMR
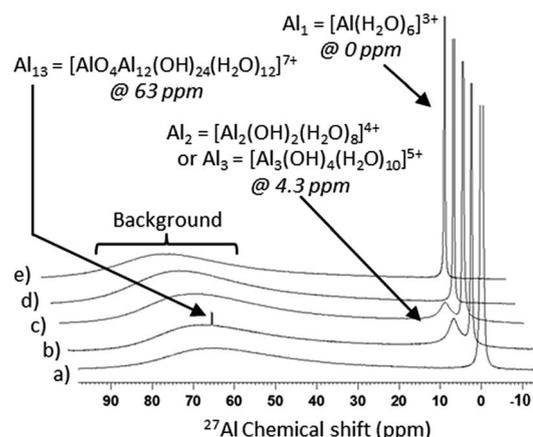

Fig. 1 ^{27}Al NMR spectra for (a) aqueous solution of $Al(NO_3)_3 \cdot 9H_2O$, [Al] = 1.6 M (b) solution of $Al(NO_3)_3 \cdot 9H_2O$ in an aqueous NaOH solution with a NaOH : Al molar ratio of 0.77 : 1 and (c–e) remnant solution after hydrothermal treatment of precursors with initial NaOH : Al molar ratio of 0.77 : 1 after 20 hour at (c) 150 °C (d) 180 °C and (e) 200 °C.
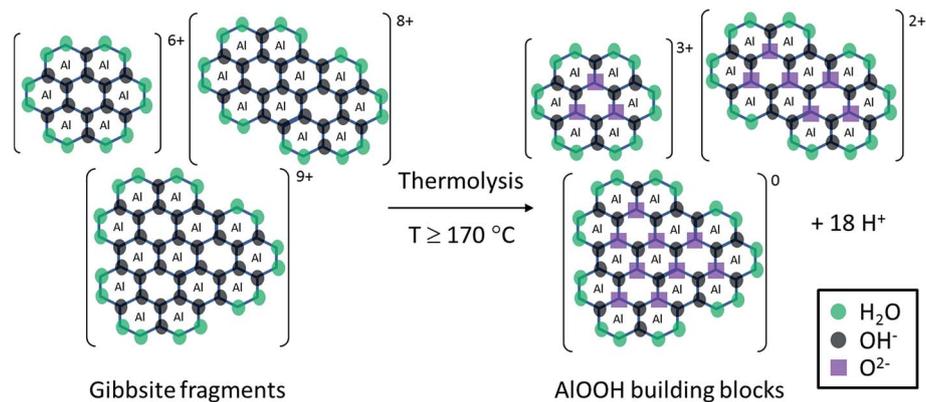
Fig. 2 Representation of the transformation of planar gibbsite fragments to AlOOH building blocks by thermolysis. Each small hexagon represents an octahedral arrangement of atoms around the Al atom. Ligands are colour coded with green, black and purple representing H_2O, OH^- and O^{2-} respectively.

(Fig. 1a), despite the fact that nitrates are believed to facilitate dimerisation.[35]

At a low NaOH : Al ratio of 0.77, corresponding to pH values <4, the aluminium species in solution tend to be monomeric and dimeric by nature.[36] Its basic hydrolysis results in the formation of Al_{13}, provided that the OH : Al ratio is between 0.5 and 2.5.[33,37] Al_{13} corresponds to a 3D tridecamer, made up of a central aluminium tetrahedron (AlO_4) surrounded by four planar trimers ($[Al_3(OH)_4(H_2O)_{10}]^{5+}$), with the chemical formula of $[Al_{13}O_4(OH)_{24}(H_2O)_{12}]^{7+}$. It is based on the structure of a Keggin cluster,[38] initially elucidated to describe the structure of heteropoly acids.[37] This structure forms because the high concentration of OH^- in the local environment during base addition yields the tetrahedral centre of $[Al(OH)_4]^-$, which is subsequently surrounded by four planar trimers ($[Al_3(OH)_4(H_2O)_{10}]^{5+}$), individually formed as per reaction (8).[39] The concentration of Al_{13} increases with slow addition of base, whereas fast base injection favours the precipitation of $Al(OH)_3$.[39] The Al_{13} species is detectable by ^{27}Al NMR (peak at 63 ppm) due to the symmetrical, tetrahedral environment of the central AlO_4. It is worth noting that the relative concentration of aluminium atoms within the Keggin cluster is 13 times higher than that shown by the area of its corresponding ^{27}Al NMR peak, as only the central tetrahedral aluminium atom is detectable by ^{27}Al NMR.[34]

As well as the formation of a complex combination of soluble aluminium species discussed so far, the addition of NaOH to aqueous solutions of aluminium nitrate also results in the formation of solid $Al(OH)_3$ *via* polymerisation. Prior to hydrothermal treatment, the initial formation of solid $Al(OH)_3$ by the addition of NaOH is limited by the OH^- concentration in the solution (reactions (3)–(6)). Thus, NaOH is the limiting reagent for the formation of AlOOH product (reaction (2))[3] after hydrothermal synthesis, despite the presence of other aluminium species in solution. Interestingly, due to the low synthesis pH, the formed $Al(OH)_3$ undergoes hydrolysis to reform soluble gibbsite fragments, whose size depends on the OH/Al ratio.[31] Indeed, we found that at pH 3.5 (OH/Al = 0.77), solid $Al(OH)_3$ fully dissolves in aqueous solution at room temperature after 48

hours. Furthermore, when the initial solution is heated to 50 °C, the solid $Al(OH)_3$ rapidly (<30 minutes) dissolves, demonstrating that, as expected, the dissolution rate increases with temperature. Consequently, under acidic hydrothermal conditions (OH/Al = 0.77), solid $Al(OH)_3$ dissolves rapidly into gibbsite fragments (pictured as reactants in Fig. 2). If the hydrothermal temperature is high enough (above 170 °C), deprotonation or hydrolysis of the gibbsite fragments by heating (thermolysis) takes place, associated with an observed decreased in pH due to the liberation of protons as depicted simplistically in Fig. 2. As deprotonation advances, the formation of relatively stable, uncharged species leads eventually to the precipitation of solid AlOOH by crystallisation.

We previously reported[3] that the amount of $Al(OH)_3$ formed determines the amount of AlOOH produced and this can now be explained as it governs the amount of gibbsite fragments which can reform in solution upon dissolution, which cannot form without base addition.

The final amount of AlOOH product formed after hydrothermal treatment during 20 hours increases as the reaction temperature is increased, as shown in Table 2. Under the studied NaOH : Al molar ratio conditions of 0.77, the maximum theoretically achievable Al_2O_3 yield is approximately 30 wt% as conversion to essential precursor $Al(OH)_3$ (reaction (3)–(6)) and subsequent gibbsite fragments, is incomplete due to the non-stoichiometric NaOH : Al ratio.[3] Such maximum conversion is only achieved after 20 hour synthesis at temperatures ≥ 200 °C, below which, the rate of conversion of gibbsite fragments into

Table 2 γ-Al_2O_3 yield following hydrothermal treatment with 1 M NaOH (0.77 NaOH : Al molar ratio) for 20 hours at different reaction temperatures

Synthesis temperature (°C)	γ-Al_2O_3 yield (wt%)
150	0
165	0
170	7
180	21
200	30

AlOOH building blocks is kinetically limited to yield less than the maximum theoretical product yield at ≤180 °C.

On the contrary, at hydrothermal temperatures ≤ 165 °C thermolysis of the gibbsite fragments (Fig. 2) is not achieved and consequently no solid product is formed as $Al(OH)_3$ is irreversibly dissolved into gibbsite fragments due to the solution acidity. Indeed, there is no change in the solution pH, confirming the absence of thermolysis reaction. The same is observed even if the synthesis is carried out for longer times (40 hours), confirming that at temperatures ≤ 165 °C, the process is not simply kinetically limited but rather it is not feasible. In addition, if this remaining solution is subsequently treated at 200 °C over 20 hours, a boehmite product is obtained with the same physical properties as boehmite synthesised by a single treatment at 200 °C for 20 hours. It is important to mention that the literature contains several studies where the synthesis of boehmite is reported at temperatures as low as 120 °C.[34,40] However, this is likely due to the different nature of aluminium and base precursors employed in these cases which undoubtedly affects the equilibria and activation energies of the intermediate synthetic steps.

The ^{27}Al NMR spectra of the supernatant solutions after hydrothermal treatment at different temperatures (Fig. 1) also show that when boehmite product is formed (≥170 °C), the dimer/trimer peak at 4.3 ppm disappears whereas it remains when no solid product is formed at ≤165 °C. This observation confirms that the dimer/trimer plays an important role in forming the final AlOOH solid product. Monomers are present in the post reaction solution, as observed by ^{27}Al NMR, after hydrothermal treatment in the studied temperature range (Fig. 1c–e) due to the non-stoichiometric NaOH : Al ratio of 0.77.
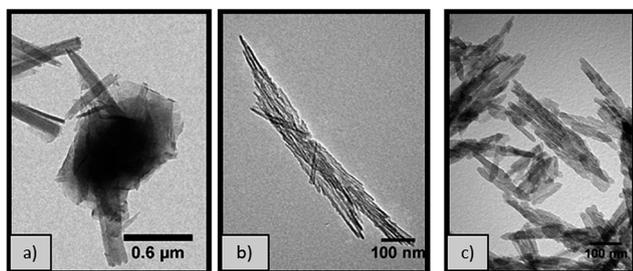
In addition, ^{27}Al NMR spectra in Fig. 1c–e show that after hydrothermal treatment at all temperatures within the studied range, the Al_{13} Keggin cluster is no longer present regardless of the formation of solid boehmite product. This suggests that the Al_{13} Keggin cluster is not directly significant for the formation of AlOOH. Indeed, the concentration of Al_{13} Keggin cluster is reported to decrease overtime in acidic conditions due to its clustering into species undetectable by ^{27}Al NMR.[34]

3.2 Mechanism of formation of 1D AlOOH nanorods

Comparison of the alumina rods produced over 20 hours with a NaOH : Al molar ratio 0.77 at different temperatures provides further insights of the formation mechanism of the boehmite structures. At temperatures ≥ 180 °C, pure nanorods are formed however, at lower temperatures (e.g. 170 °C), a variety of morphologies, including 2D rectangular nanoplates and nanoparticles, are observed (Fig. 3a). This is due to the lower rate of conversion of these intermediate products into the more thermodynamically stable nanorods via scrolling followed by oriented attachment (Fig. 8). This scrolling step forming nanorods from lamellar sheets does not take place at 170 °C, while it is kinetically limited at 180 °C, as shown by the low aluminium yield obtained (Table 2). In all cases, the pXRD pattern (Fig. S1†) of the calcined boehmite materials (500 °C) can be indexed to the γ phase of Al_2O_3 (JCPDS card no. 10-0425), without the presence of other crystalline phases. Additionally, the materials produced at temperatures ≥ 180 °C present similar BET surface areas (~145 m² g⁻¹), irrespective of the distinct nanorod dimensions shown by TEM (Fig. 3b and c). By contrast, the alumina material produced under the same conditions at 170 °C has a lower BET surface area (122 m² g⁻¹), likely due to the difference in morphology (Fig. 3a) and porosity (Fig. S5†).

Table 3 shows that as the synthesis temperature increases, the crystallite size increases. Interestingly, a 10 °C increase from 170 to 180 °C results in doubling of the crystallite size in both (440) and (400) directions whereas a 20 °C increase from 180 °C to 200 °C only results in a <1 nm increase in size due to higher rate of crystallite formation as temperature increases. Additionally, rod formation is not observed at 170 °C, while it is the principal morphology obtained at higher temperatures.

For the samples synthesised at 180 °C and 200 °C, the crystallite size in both the (400) and the (440) direction is of comparable size of 6 to 7 nm. However, SEM micrographs in

Fig. 3 TEM micrographs of γ-Al_2O_3 obtained from hydrothermal treatment for 20 hours with 1 M NaOH (0.77 NaOH : Al molar ratio) at (a) 170 °C (b) 180 °C and (c) 200 °C.

Table 3 Properties of γ-Al_2O_3 materials synthesised at 170, 180 and 200 °C for 20 hours (0.77 NaOH : Al molar ratio)

Synthesis temperature (°C)	Morphology	SA_{BET}[a] (m² g⁻¹)	Average crystallite size[b] (nm)	
			(440)	(400)
170	Rectangular sheets and nanoparticles	122	3.1	2.9
180	Rods	144	6.4	6.1
200	Rods	146	7.1	6.8

[a] SA_{BET}: specific surface area calculated using the BET approximation using N_2 sorption data at −196 °C. [b] Calculated from line broadening at half maximum intensity of (440) and (400) XRD peaks using the Scherrer equation.

Fig. 4 show that the nanorods synthesised at 180 °C are longer and thinner than those synthesised under comparable conditions at 200 °C. It is important to mention that the samples were coated with a thin layer of platinum to reduce charging and consequently quantitative analysis of these micrographs is not applicable. High resolution TEM analysis of the material synthesised for 20 hours at 200 °C (Fig. 5) confirms that the rods consists of attached crystallites, in agreement with the small crystallite size calculated by pXRD (Table 3). The individual crystallites aggregate by the oriented attachment mechanism.

The mechanism of oriented attachment is driven by the presence of NO_3^- anions in the solution which stabilise specific AlOOH surfaces, inhibiting the growth in that direction. Specifically, NO_3^- anions bind to the AlOOH surface through the surface hydroxyl groups which are protonated in acidic conditions to $-OH_2^+$, making it capable of attracting a negative ion.[24] This effect can be tuned by controlling the adsorption strength of the anion and their complexing ability with Al^{3+}, following the order $SO_4^{2-} > Cl^- > NO_3^-$, whereby SO_4^{2-} presents the strongest growth promotion in the direction where no adsorption interaction is possible.[24] Interestingly, poor crystallinity and the formation of short nanorods (aspect ratio 2–4) have been reported elsewhere with NO_3^-, which may due to the morphology directing polymer employed.[1] This is contrary to our observations, likely due to the fact that our synthesis does not use a structure directing agent.

3.3 Nanorod growth

In order to fully understand the reasons behind the different nanorod dimensions observed in Fig. 3b and c and consequently
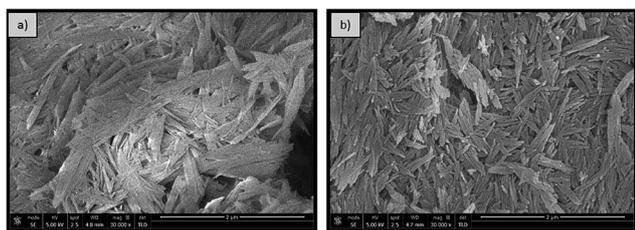

Fig. 4 SEM micrographs of γ-Al_2O_3 nanorods synthesised for 20 hours with 1 M NaOH (0.77 NaOH : Al molar ratio) at (a) 180 °C and (b) 200 °C.
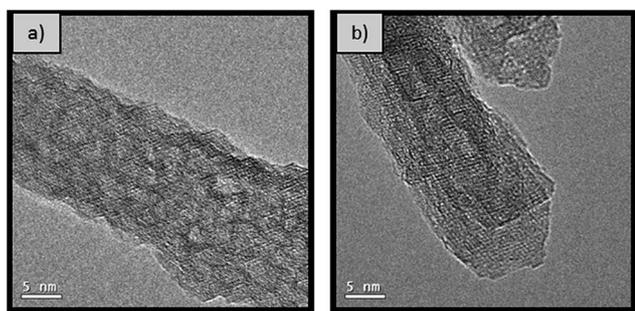

Fig. 5 High resolution TEM micrograph of nanorods synthesised with 1 M NaOH (0.77 NaOH : Al molar ratio) at 200 °C for 20 hours (a) before and (b) after calcination at 500 °C.

the effect of temperature on the size of the rods, a series of hydrothermal syntheses were carried out at 180 °C and 200 °C for different durations from 10 to 80 hours. Fig. 6 shows representative TEM micrographs of the materials. All of the samples show high morphological purity, except the sample synthesised at 180 °C for 10 hours (Fig. 6a) where nanorods are not formed but rather a mixture of morphologies, including sheets and nanoparticles, are observed, resembling the sample synthesised at 170 °C for 20 hours (Fig. 3a). This observation confirms that the scrolling of the AlOOH sheets, taking place under acidic conditions[3] herein, is kinetically limited at such low temperatures.

Careful characterisation of the samples also reveals the presence of two distinct products formed at 180 °C, including rods with a high aspect ratio (>40), mixed with considerably lower aspect ratio (<17) rods. This is clearly illustrated by the bimodal length and diameter size distribution (Fig. S2†). Both products are separated by post-synthesis sedimentation; the high aspect ratio rods have high surface energy and aggregate, falling to the bottom of the autoclave while the low aspect ratio rods remain in suspension and are collected using centrifugation. Histograms of the lengths and diameters are shown in the ESI (Fig. S2†), with average values summarised in Table 4. The pXRD patterns (Fig. S3 and S4†) of the materials in Fig. 6 show the presence of a single crystalline phase corresponding to γ-Al_2O_3 (JCPDS card no. 10-0425).

As shown in Table 4, similar surface areas are observed for γ-Al_2O_3 nanorods synthesised for 20 hours at 180 °C and 200 °C despite the difference in size of the low aspect ratio nanorods. This is likely due to the sample produced at 180 °C containing both low and high aspect ratio nanorods, the later has a higher surface area, thus increasing the average surface area of the sample. Despite the variability of nanorod dimensions as the hydrothermal duration changes, all samples produced at 200 °C present a similar aspect ratio (~10), suggesting a multi-directional nature of the dissolution–recrystallisation mechanism.

All the samples summarised in Table 4 are mesoporous with a characteristic type IV N_2 sorption isotherm with hysteresis (Fig. S5†). Additionally, all nanorods produced, independently of the synthesis time, present a similar crystallite size (~5–7 nm), calculated using the Scherrer equation with the line broadening at half maximum intensity of the (440) and (400) diffraction peaks. The high resolution TEM micrographs shown in Fig. 5 further confirms that the rods are indeed formed by agglomeration of crystals, via the oriented attachment of AlOOH nanorod crystallites formed by scrolling of AlOOH sheets.

Rods with high aspect ratio (long and thin) are formed by oriented attachment of the scrolled crystallites formed under acidic conditions. Once the 1D high aspect boehmite nanorods have been formed, they are susceptible to growth via Ostwald ripening[41] following a dissolution/recrystallisation mechanism, which has been observed in other 1D ceramic structures.[42] This growth step takes place simultaneously with further rod formation, leading to the bimodal size distribution observed for the samples synthesised at 180 °C. In addition, due to the formation and growth steps taking place simultaneously, the narrow diameter and length size distribution achieved after 10
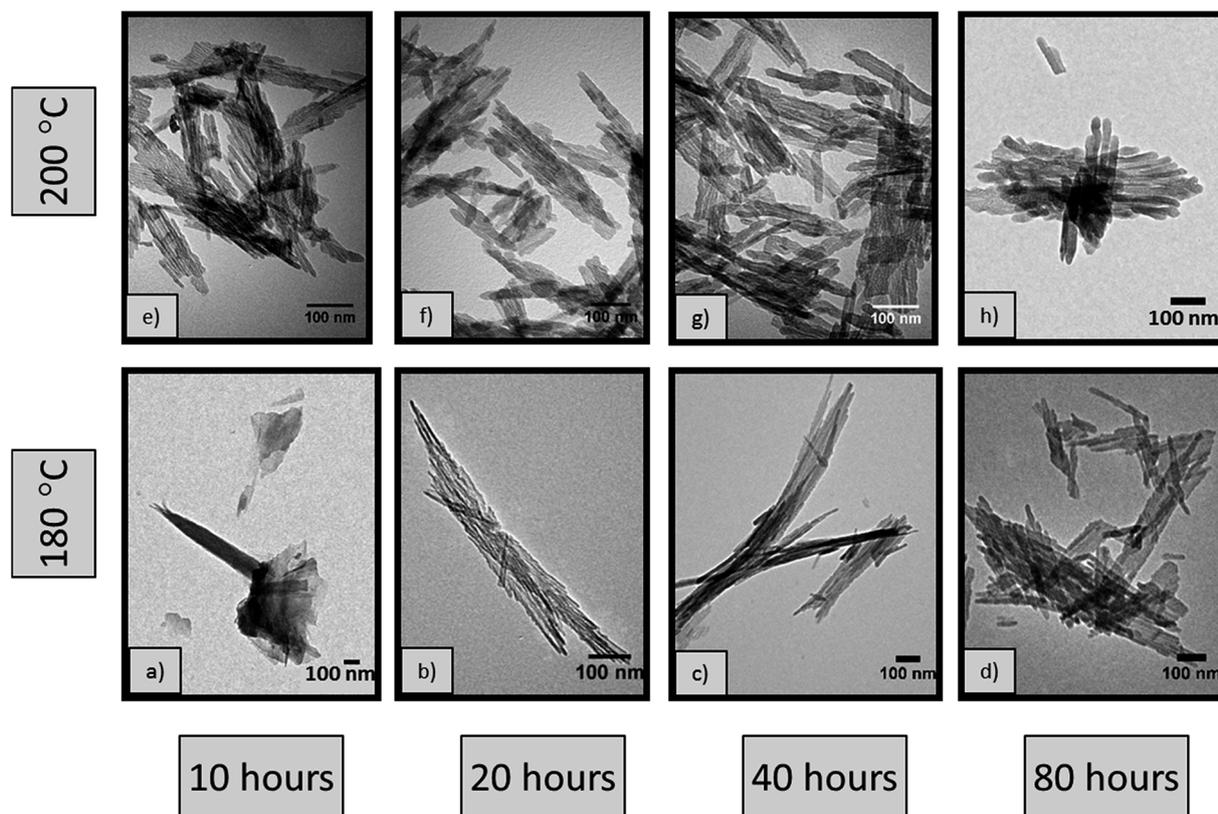
Fig. 6 TEM micrographs of γ-Al_2O_3 synthesised with 1 M NaOH (0.77 NaOH : Al molar ratio) at 180 °C for (a) 10 hours (b) 20 hours (c) 40 hours (d) 80 hours and at 200 °C for (e) 10 hours (f) 20 hours (g) 40 hours (h) 80 hours.

Table 4 Physical properties of γ-Al_2O_3 nanorods synthesised at 180 °C and 200 °C for 10 to 80 hours[a]

Temperature (°C)	Synthesis time (hours)	Average length (nm)	Average diameter (nm)	Aspect ratio[b]	SA$_{BET}$[c] (m^2 g^{-1})	Average crystallite size[d] (nm)		Yield (wt%)
						(440)	(400)	
180 °C	10	N/A	N/A	N/A	117	2.6	50.1	11
	20	115	8	14	144	6.4	6.1	21
		318	*5*	*64*				
	40	133	11	12	147	5.1	4.8	28
		287	*7*	*41*				
	80	213	18	12	123	5.9	5.8	23
		518	*13*	*40*				
200 °C	10	80	8	10	161	6.5	5.9	20
	20	128	13	10	146	7.1	6.8	30
	40	182	20	9	86	6.9	6.4	25
	80	290	26	11	106	7.3	6.4	15

[a] γ-Al_2O_3 synthesised at 180 °C and 200 °C with 1 M NaOH (0.77 NaOH : Al molar ratio). Data for high aspect ratio rods shown in italics. [b] Length : diameter ratio. [c] SA$_{BET}$: specific surface area calculated using the BET approximation using N_2 sorption data at −196 °C. [d] Calculated with Scherrer equation using line broadening at half maximum intensity of (440) and (400) XRD peaks.

hours of synthesis, gets broader as the hydrothermal time is increased to 80 hours. At 200 °C, the rate of both steps is increased, resulting not only in a monomodal length and diameter size distribution, but also in rods with smaller aspect ratios. The increased rate of scrolling and oriented attachment of AlOOH crystallites forming rods at 200 °C compared to 180 °C is evidenced by the higher aluminium yields achieved in the former case for a given synthesis time (Table 4). Furthermore, the ease of growth by dissolution–recrystallisation depends on the degree of solubility of the crystallites,[27] which increases as
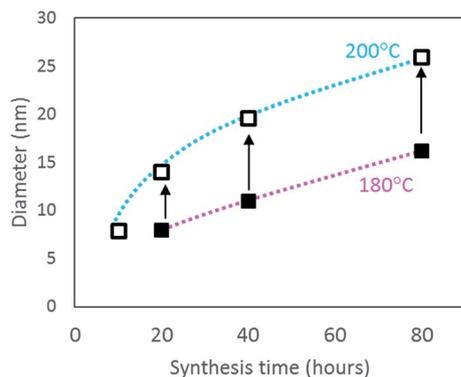
Fig. 7 Variation in diameter of low aspect ratio nanorods following increased synthesis time (10 to 80 hours) at 180 °C (closed square) and at 200 °C (open square).

the temperature increases, leading to a higher growth rate at 200 °C compared to 180 °C. This is evidenced in Table 4 and Fig. 7 as the diameter for the low aspect rods synthesised at 200 °C are larger than the equivalent material produced for the same time but at 180 °C. This is in agreement with previous observations by Xu *et al.*[40] who reported an increase in the diameter and length of the rods with increasing reaction temperature from 120 to 180 °C.

In addition, the length and diameter of the rods is increased by extending the synthesis time as shown in Fig. 7 for the low aspect nanorods. One should notice that the average diameter of the low aspect ratio rods produced after 20 hours at 180 °C is similar to the diameter of the nanorods produced after only 10 hours at 200 °C. Since nanorods are not formed after 10 hours at 180 °C, no data point is included in Fig. 7. These observations demonstrate that low aspect ratio nanorods with similar dimensions can be produced at 200 °C for shorter synthesis time (10 hours) than at 180 °C with double synthesis time (20 hours). In the latter case, the rods will be simultaneously produced with high aspect ratio rods, which can be separated by sedimentation as mentioned previously.

Based on the systematic study presented herein, the overall process for the hydrothermal synthesis of nanorods in acidic conditions has been elucidated, revealing a six step mechanism, summarised in Fig. 8. Initially, NaOH addition to an aqueous solution of $Al(NO_3)_3 \cdot 9H_2O$ forms $Al(OH)_3$ (step 1), which undergoes hydrolysis into fragments of gibbsite due to the acidic conditions (step 2). At a hydrothermal temperature $\geq$ 170 °C, thermolysis (step 3) takes place to yield AlOOH building blocks that subsequently crystallise into lamellar sheets of AlOOH, (step 4), evidenced by TEM analysis of the product obtained after hydrothermal treatment at 170 °C. The formation of nanorods (step 5) proceeds only at $\geq$180 °C for 20 hours, involving scrolling to form nanorods crystallites which can attach in an oriented way to form high aspect ratio nanorods. At higher temperatures (200 °C), step 5 can be achieved after a shorter hydrothermal treatment time of 10 hours. These nanorods can grow (step 6) in a non-selective, multi-directional manner by Ostwald ripening, resulting in low aspect ratio (<20) nanorods. At 200 °C, step 5 is sufficiently fast that only low aspect ratio nanorods are observed, whereas 180 °C results in a mixture of low and high aspect ratio nanorods.

4. Conclusion

In conclusion, a systematic study of the effect of temperature and time on the hydrothermal synthesis of γ-Al_2O_3 nanorods is presented here, revealing an in-depth understanding of the formation mechanism. Herein, we have presented and discussed an evidence based six-step mechanism, taking into account all aspects of the process. The formation of $Al(OH)_3$ (step 1) and its consequent dissolution into hexameric gibbsite fragments (step 2) takes place before hydrothermal treatment. This is followed by thermolysis into AlOOH blocks (step 3) followed by lamellar AlOOH formation (step 4), their scrolling and oriented attachment to form AlOOH rods (step 5) and their simultaneous growth (step 6). Electron microscopy, ^{27}Al NMR studies and experimental observations demonstrate that the reaction temperature plays a key role in the formation of nanostructured AlOOH. A
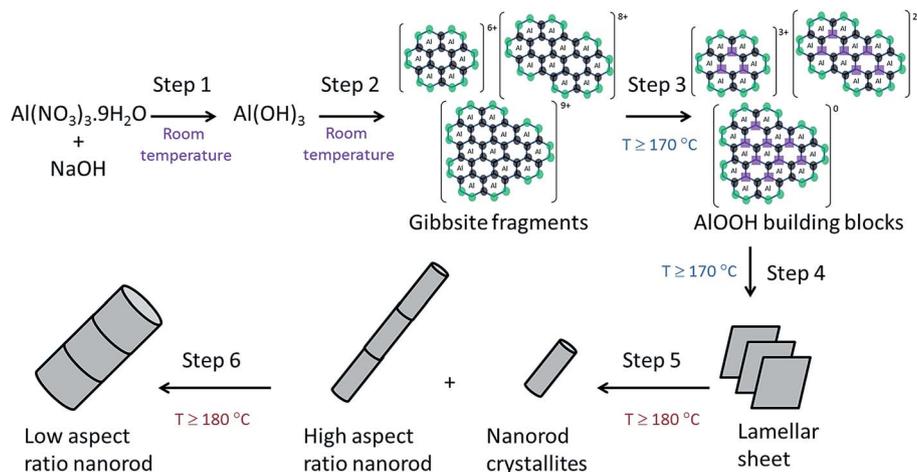

Fig. 8 Summary of the elucidated six step mechanism for nanorod formation by hydrothermal synthesis under acidic conditions.

minimum hydrothermal temperature of 170 °C is needed to form AlOOH (step 4) but a higher temperature of 180 °C is needed to form AlOOH nanorods (step 5). Understanding the relative rate of steps 4–6 at different temperatures allows for control of the nanorod dimensions. We, thus, demonstrate that γ-Al$_2$O$_3$ nanorods of selective diameter and length can be synthesised by varying the hydrothermal treatment time and temperature. The nanorod diameter can be increased by raising the hydrothermal temperature from 180 °C to 200 °C or by prolonging the synthesis time up to 80 hours *via* growth by Ostwald ripening (step 6). However after 80 hours synthesis, the nanorod size distribution is considerably broader, losing size control.

Acknowledgements

References

1 W. Cai, Y. Hu, J. Chen, G. Zhang and T. Xia, *CrystEngComm*, 2012, **14**, 972–977.

2 M. Trueba and S. P. Trasatti, *Eur. J. Inorg. Chem.*, 2005, **2005**, 3393–3403.

3 T. E. Bell, J. M. Gonzalez-Carballo, R. P. Tooze and L. Torrente-Murciano, *J. Mater. Chem. A*, 2015, **3**, 6196–6201.

4 Q. Yang, *Inorg. Mater.*, 2010, **46**, 953–958.

5 Y. X. H. Hou, Q. Yang, Q. Guo and C. Tan, *Nanotechnology*, 2005, **16**, 741–745.

6 M.-G. Ma, Y.-J. Zhu and Z.-L. Xu, *Mater. Lett.*, 2007, **61**, 1812–1815.

7 H. C. Lee, H. J. Kim, S. H. Chung, K. H. Lee, H. C. Lee and J. S. Lee, *J. Am. Chem. Soc.*, 2003, **125**, 2882–2883.

8 Z. Zhang and T. J. Pinnavaia, *Langmuir*, 2010, **26**, 10063–10067.

9 L. Qu, C. He, Y. Yang, Y. He and Z. Liu, *Mater. Lett.*, 2005, **59**, 4034–4037.

10 H. A. Dabbagh, K. Taban and M. Zamani, *J. Mol. Catal. A: Chem.*, 2010, **326**, 55–68.

11 T. Kim, J. Lian, J. Ma, X. Duan and W. Zheng, *Cryst. Growth Des.*, 2010, **10**, 2928–2933.

12 B. Xu, T. Xiao, Z. Yan, X. Sun, J. Sloan, S. L. González-Cortés, F. Alshahrani and M. L. H. Green, *Microporous Mesoporous Mater.*, 2006, **91**, 293–295.

13 Y. Zhang, J. Liu, R. He, Q. Zhang, X. Zhang and J. Zhu, *Chem. Phys. Lett.*, 2002, **360**, 579–584.

14 M. Sasani Ghamsari, M. A. Abdul-Hamid, S. Radiman, A. H. Sasani Ghamsari and S. Rahmani, *Mater. Lett.*, 2013, **106**, 439–442.

15 S. C. Kuiry, E. Megen, S. D. Patil, S. A. Deshpande and S. Seal, *J. Phys. Chem. B*, 2005, **109**, 3868–3872.

16 F. Rashidi, A. N. Kharat, A. M. Rashidi, E. Lima, V. Lara and J. S. Valente, *Eur. J. Inorg. Chem.*, 2010, **2010**, 1544–1551.

17 J. N. D. de Leon, V. Petranovskii, J. A. de los Reyes, G. Alonso-Nunez, T. A. Zepeda, S. Fuentes and J. L. Garcia-Fierro, *Appl. Catal., A*, 2014, **472**, 1–10.

18 L. Pu, X. Bao, J. Zou and D. Feng, *Angew. Chem., Int. Ed.*, 2001, **40**, 1490–1493.

19 J. Zou, L. Pu, X. Bao and D. Feng, *Appl. Phys. Lett.*, 2002, **80**, 1079–1081.

20 L. Yi, L. Zhiyuan, H. Xing, L. Yisen and C. Yi, *Chem. Commun.*, 2011, **47**, 2173–2175.

21 J. S. Lee, B. Min, K. Cho, S. Kim, J. Park, Y. T. Lee, N. S. Kim, M. S. Lee, S. O. Park and J. T. Moon, *J. Cryst. Growth*, 2003, **254**, 443–448.

22 J. Hwang, B. Min, J. S. Lee, K. Keem, K. Cho, M. Y. Sung, M. S. Lee and S. Kim, *Adv. Mater.*, 2004, **16**, 422–425.

23 Z. Zhu, H. Sun, H. Liu and D. Yang, *J. Mater. Sci.*, 2010, **45**, 46–50.

24 T. He, L. Xiang and S. Zhu, *CrystEngComm*, 2009, **11**, 1338–1342.

25 Y. Z. M. Ma, G. Cheng and Y. Huang, *J. Mater. Sci. Technol.*, 2008, **24**, 637–640.

26 S. C. Shen, Q. Chen, P. S. Chow, G. H. Tan, X. T. Zeng, Z. Wang and R. B. H. Tan, *J. Phys. Chem. C*, 2006, **111**, 700–707.

27 P. Pardo, N. Montoya and J. Alarcon, *CrystEngComm*, 2015, **17**, 2091–2100.

28 J. Wang, K. Shang, Y. Guo and W.-C. Li, *Microporous Mesoporous Mater.*, 2013, **181**, 141–145.

29 S. Ghosh, R. Das and M. K. Naskar, *J. Am. Ceram. Soc.*, 2016, **99**, 2273–2282.

30 Y.-F. Han, Z. Zhong, K. Ramesh, F. Chen and L. Chen, *J. Phys. Chem. C*, 2007, **111**, 3163–3170.

31 S. Bi, C. Wang, Q. Cao and C. Zhang, *Coord. Chem. Rev.*, 2004, **248**, 441–455.

32 G. Fu, L. F. Nazar and A. D. Bain, *Chem. Mater.*, 1991, **3**, 602–610.

33 S. M. Bradley, R. A. Kydd and R. F. Howe, *J. Colloid Interface Sci.*, 1993, **159**, 405–412.

34 R. J. M. J. Vogels, J. T. Kloprogge, P. A. Buining, D. Seykens, J. B. H. Jansen and J. W. Geus, *J. Non-Cryst. Solids*, 1995, **191**, 38–44.

35 C. V. Ruiz Madroñero and J. E. Rodríguez Paéz, *Ing. Invest.*, 2010, **30**, 16–24.

36 H. Zhao, H. Liu and J. Qu, *J. Colloid Interface Sci.*, 2009, **330**, 105–112.

37 G. Furrer, C. Ludwig and P. W. Schindler, *J. Colloid Interface Sci.*, 1992, **149**, 56–67.

38 J. F. Keggin, *Nature*, 1933, **131**, 908–909.

39 J. T. Kloprogge, D. Seykens, J. B. H. Jansen and J. W. Geus, *J. Non-Cryst. Solids*, 1992, **142**, 94–102.

40 X. Xu, Y. Liu, Z. Li, Z. Lv, J. Song, M. He, Q. Wang, L. Yan and Z. Li, *J. Therm. Anal. Calorim.*, 2014, **115**, 1111–1117.

41 L. Zhang, X. Jiao, D. Chen and M. Jiao, *Eur. J. Inorg. Chem.*, 2011, **2011**, 5258–5264.

42 L. Torrente-Murciano, A. A. Lapkin and D. Chadwick, *J. Mater. Chem.*, 2010, **20**, 6484–6489.